

Study of Copper Adsorption on Montmorillonites using Thermal Analysis Methods

Zhe Ding* and Ray L. Frost

*Inorganic Materials Research Program, School of Physical and Chemical Sciences,
Queensland University of Technology,
2 George Street, GPO Box 2434, Brisbane, Qld 4001, Australia*

Copyright 2004 Elsevier

Published as:

Z. Ding, and L. Frost Ray, Study of copper adsorption on montmorillonites using thermal analysis methods. Journal of colloid and interface science, 2004. 269(2): p. 296-302.

Abstract

Copper was adsorbed onto Ca-exchanged montmorillonite (Cheto clay) under basic conditions. Differential Thermogravimetric Analysis (DTG) combined with evolved gas Mass Spectroscopy (MS) was employed as the principal technology to study the distribution and structure of adsorbed copper species on a montmorillonitic clay. The results showed that the original clay was easily rehydrated. After copper adsorption, a step-by-step replacement of hydrated calcium ions by copper-ammonia complex was observed through the gradual decrease of the first DTG dehydration peak intensity with increasing copper loading. Compared with the original clay, copper loaded samples showed new DTG peaks assigned to NH_3 and N_2O . The presence of N_2O peak suggested that the loaded copper species were in agglomerated copper oxide form, which dispersed well over the edges and external surfaces of the clay layers.

Introduction

Adsorption of metal ions onto clay minerals has been studied extensively because both metal ions and clays are common components in nature and also because a knowledge of the adsorption process could aid in the environmental remediation of water that is polluted by heavy metal ions.

From our point of view, copper is of particular interest, because of its catalytic performance in the reactions such as wet air oxidation (WAO) [1-6] for wastewater treatment and selective catalytic reduction (SCR) of NO_x [7-9]. Copper has been loaded onto different supports and used as catalysts in these reactions [7-9]. The most explored support materials are zeolite [9], alumina [2, 3] and titania [8]. There are few reports using clays as supports for such applications and there is little information about the structure of different clay supported copper phases. Considering the large deposits of clay minerals, it is economically favourable to use clays as catalyst supports. Previous studies showed promising catalytic performances for copper loaded pillared clays in WAO [10, 11] and SCR [12-14] reactions. In these works, generally, before copper adsorption, clay was modified by pillaring processes to enhance

* Corresponding author. Tel: +61-7-3864 1220. Fax: +61-7-3864 1804. E-mail: z.ding@qut.edu.au

surface area and porosity [13, 15, 16]. The catalytic reaction results showed that the amount and state of the adsorbed copper species was critical for the catalytic activities. Therefore, it is worthwhile to apply raw clays as support materials. The focus of this study is to investigate the adsorption of copper onto clays and their structures under different synthesis conditions. For the first time, combined DTG-MS technique was used to distinguish the different locations of the adsorbed copper species on the clay surface.

Experimental

Sample preparation

The starting clay material was Cheto montmorillonite (from Clay Minerals Repository, University of Missouri-Columbia). It was mainly Ca-exchanged montmorillonite and used as received without any additional treatment.

Copper adsorption was conducted under basic conditions. To 0.01 M of copper nitrate solution, ammonium hydroxide solution (5%) was added to adjust the pH to 12. The resulting solution was deep blue colour, indicating the formation of the $[\text{Cu}(\text{NH}_3)_4]^{2+}$ complex [17]. Various amounts of this copper solution was added to 5 wt% of clay suspension with Cu / clay ratios of 0.2, 0.5 and 1 mmol/g, respectively. The resulting suspension was stirred for 18 h, followed by separation, washing and drying slowly at 80 °C. The obtained samples were labelled as Cu/Cheto-n, where n = 1, 2, and 3 to represent different Cu / clay ratios.

Characterization

DTGA-MS was conducted on TA[®] Instruments Thermogravimetric Analyser (TGA, Q500) equipped with an Evolved Gas Analysis (EGA) Furnace, which was connected to a Quadrupole Mass Spectrometer (PFEIFFER, QMS 200 Prisma) through a 1/8 inch, in diameter, transfer line. Nitrogen was used as the purging gas and the flow rate was controlled precisely at 80 mL/min. Around 50 mg of sample powders were loaded onto platinum sample pan and the analysis was performed under two conditions. A normal ramp procedure was used for condition I. Sample was preheated to 30 °C and isothermal for 10 min, then it was heated to 900 °C at a heating rate of 4 °C/min. A controlled rate thermal analysis (CRTA) was used for condition II. The sample was heated to 900 °C at a heating rate of 10 °C/min, where the heating rate was dynamically and continuously modified according to the changes in the rate of the sample weight loss.

X-ray diffraction (XRD) patterns of the samples were collected on ENRAF NONIUS DELFT DIFFRACTIS 583, using cobalt K_{α} radiation. Sample powders were calcined at 400 °C for 5 h and XRD measurements were performed on both the calcined and freshly prepared samples. Each XRD scan was obtained at a speed of 1 °/min with step size of 0.02 °.

X-ray photoelectron spectroscopy (XPS) analysis was conducted on a PHI model 560 XPS/SAM/SIMS I multitechnique surface analysis system. The X-ray source was provided by the monochromatic Mg K_{α} radiation, which was operated at 15 kV. Powders were loaded onto sample holder by double face sticky tape. Since the thickness of single clay layer is around 9.8 Å and XPS can detect surface information within depth of 60 Å. Therefore, the element concentrations obtained from XPS measurement were treated as the bulk concentrations.

UV-Vis Diffuse reflectance spectra (DRS) for calcined samples were collected at room temperature on a Varian-Cary 100 Conc UV-vis spectrophotometer with a diffuse

reflectance accessory. The Schuster-Kubelka-Munk function ($F(R)=(1-R_{\infty})^2/2R_{\infty}$) was calculated and plotted against the wavelength.

Results and discussion

Fig. 1.

Fig. 1 shows the XRD patterns of the original Cheto clay and different Cu/Cheto-n samples before and after calcination. By comparison with the XRD patterns for the original Cheto clay in Fig. 1 (a) and (b), it is clear that there is little variation in the first diffraction (*001*) peak position after calcination. The calculated d-spacings, as shown in the figure, are 1.55 nm and 1.58 nm, respectively. Although the fresh Cheto clay has much better peak shape and higher peak intensity, the appearance of the *001* peak at the similar position indicates that Cheto clay rehydrates easily. To verify this finding, a further measurement was conducted on Cheto clay only. After the calcination, instead of being compressed into sample holder, Cheto clay powders were quickly dispersed and affixed onto glass slides by Vaseline to minimise the amount of water vapour adsorbed during the preparation. XRD analysis was undertaken on the same glass slide, which was exposed to air for different periods of time. The results are shown in Fig. 2.

Fig. 2.

It is seen that for Cheto clay after exposure to air for 0.5 h, no peak can be observed, except a broad, nearly invisible hump around 10.5° of 2θ . Such a hump has vanished after exposure to air for 1h. In addition, there is an obvious gradual increase of another peak around 6.5° of 2θ . Compared with the *001* peak for uncalcined Cheto clay, it is clear that this peak with increasing intensity is coming from the expanded clay layers after water vapour adsorption. Therefore, Ca-exchanged montmorillonite (Cheto clay) is easily rehydrated.

After copper adsorption, as shown in Fig. 1 (a) and (b), compared with Cheto clay, there is a decrease of the d-spacings for both samples before and after calcination. Furthermore, there is not much difference among the three Cu/Cheto-n samples, except that Cu/Cheto-1 shows slightly higher d-spacing. Contrary to what happened to the original Cheto clay, a general shift of the *001* peak to the lower d-spacing after calcination is observed. This implies that Ca is replaced by the Cu species and the latter does not rehydrate after being calcined. One would expect that these exchanged Cu species sitting in-between the clay layers. However, it is difficult to determine from XRD results only, as there is little increase in the d-spacing. Considering the thickness of the single clay layer, which is 0.98 nm, it is clear that there is no layer expansion after copper loading. A slightly higher d-spacing for Cu/Cheto-1 might come from the agglomerated copper species sitting in-between the layers, or might come from the incomplete exchange of Ca by Cu.

The bulk element concentrations determined from XPS analysis are summarised in Table 1.

Table 1.

It is observed that the amount of loaded copper is proportional to the starting Cu / Clay ratio during the synthesis and it seems would reach a plateau if the Cu / Clay ratio was increased to higher than 1 mmol / g. In addition, for Cu/Cheto-1, there is still 2.0 wt% CaO after copper exchange, which is reduced to 0.55 wt% for Cu/Cheto-2. Therefore, the higher d-spacing in XRD analysis for Cu/Cheto-1 compared with the other two samples is more likely to come from the rehydration of those un-exchanged Ca ions. Apart from the characteristic

peaks assigned to montmorillonite clay, no other peaks are detected for any types of copper crystallite phases.

The normal ramping DTGA-MS results for original Cheto clay and Cu/Cheto-n, using Cu/Cheto-2 as representative, are illustrated in Fig. 3 and Fig. 4, respectively.

Fig. 3 and Fig. 4.

From Fig. 3, it is seen that the starting Cheto clay has two main weight loss regions, (i) below 200 °C, and (ii) between 500 – 700 °C. The on-line MS analysis shows that only water, as observed by masses 18 and 17, is generated during the sample heating and the MS data follows precisely the same trend as that of DTG data. Therefore, Cheto clay has two dehydration peaks centred at 63 °C and 125 °C, region (i), and one broad dehydroxylation peak centred at 608 °C, region (ii). Such a result is typical for montmorillonite clays, which upon heating, surface adsorbed water is lost first. Further heating will cause the rupture of the structural hydroxyl groups, leading to the dehydroxylation peak at higher temperature. It is proposed that the dehydroxylation process is partially non-reversible, where the layered structure collapses. However, ads./desorption of water is reversible. From Fig. 3, it is clear that the dehydroxylation only happens when the temperature is over 500 °C. This supports the results obtained from XRD analysis, as shown in Fig. 2, that the calcination temperature (400 °C) is not high enough to destroy the layered structure and the clay is easily rehydrated.

For the Cu/Cheto-n samples, as shown in Fig. 4, four main weight loss regions are observed, (i) below 150 °C, (ii) between 150 °C and 350 °C, (iii) between 350 °C and 700 °C, and (iv) between 800 °C and 870 °C. In addition, more signals have been picked up during the on-line MS analysis, including mass 16, 17, 18, 32, and 44. Because the copper adsorption was conducted under basic condition by adding ammonium hydroxide solution, the major adsorption species would be $[\text{Cu}(\text{NH}_3)_4]^{2+}$. Therefore, in the MS results, mass 16 is assigned to ammonia, mass 18 to water, while mass 17 can be attributed to either water or ammonia. Mass 32 is oxygen, which appears at fairly high temperatures, indicating the restructure of the adsorbed copper species. The presence of mass 44 is not anticipated. The first thought is to assign it to CO_2 , which is coming from the organic impurity in Cheto clay. However, mass 44 was not detected in the MS analysis for original Cheto clay, which excludes such a possibility. Considering that the TGA analysis was performed under the nitrogen conditions, it is likely that mass 44 is not a result of the pure weight loss, but a reaction between the sample and nitrogen as follows:



or



Therefore, mass 44 is assigned to N_2O . By combining MS data with DTG data, it is proposed that Cu/Cheto-2 undergoes the following steps during heating. In region (i), mainly water is desorbed with a dehydration peak centred at 65 °C. More water is released in region (ii), centred at 250 °C, and region (iii), centred at 510 °C and 610 °C. Compared with the original Cheto clay, the dehydration peak at 125 °C disappears and Cu/Cheto-2 has new dehydration peaks at 250 °C and 510 °C, which are related to the water associated with the adsorbed copper species. In addition, Cu/Cheto-2 has the similar dehydroxylation peak (610 °C) to that of the original Cheto clay. In the same regions (ii) and (iii), ammonia is also released with peaks centred at 300 °C and 470 °C. Therefore, adsorbed copper species are located on at least two different types of sites. Furthermore, at the end of region (iii), N_2O is

produced, with the peak centred at 650 °C. In region (iv), only oxygen is released with the peak centred at 865 °C.

A comparison of DTGA curves for different Cu/Cheto-n samples is given in Fig. 5.

Fig. 5.

It is seen that Cu/Cheto-1 and 3 have the similar DTGA pattern as that of Cu/Cheto-2. In region (i), Cu/Cheto-1 shows the highest dehydration peak, followed by Cu/Cheto-2 and Cu/Cheto-3. In addition, Cu/Cheto-1 has a shoulder around 130 °C, similar position as the second dehydration peak for the original Cheto clay. As discussed before, Cheto clay has exchangeable hydrated calcium ions. After treatment with copper solution, these hydrated calcium ions are replaced by copper ions. Since copper ions were surrounded by ammonia, after copper adsorption, less water is adsorbed onto the clay surface. Therefore, the first dehydration peak intensity decreases. Fig. 5 clearly reflects the step-by-step exchanging of calcium ions by copper ions. The exception is the shoulder for Cu/Cheto-1 coming from the least exchanging extent for Cu/Cheto-1, which agrees well with the above XRD and XPS results.

The weight loss in region (ii) is dominated by ammonia. Although clay itself also adsorbs ammonia, it is believed that the ammonia is introduced into the clay structure mainly through the adsorbed $[\text{Cu}(\text{NH}_3)_4]^{2+}$ complex. If this is true, the amount of ammonia desorbed during TGA analysis should be closely related to the amount of copper loaded. From Fig. 5, it is seen that in this region, the peak intensities follow the trend Cu/Cheto-3 > Cu/Cheto-2 > Cu/Cheto-1, which is the same order as those of the copper concentrations listed in Table 1. Therefore, DTG results in regions (i) and (ii) demonstrate the replacement of the hydrated calcium ions by copper complex and the proportional relationship between the loading rate and the initial Cu / Cheto ratio.

The weight loss in region (iii) is more complicated, because of the contributions from NH_3 , H_2O and N_2O with the increasing temperature. As discussed above, the simultaneous occurrence of NH_3 and H_2O around 500 °C indicates that copper complex is adsorbed on different sites of clay surface. The peak intensity for NH_3 is much weaker in region (iii) than in region (ii), which implies that much less copper complex is adsorbed on this second type of sites. In addition, there is only a slight difference in the peak intensities among three samples, with the order of Cu/Cheto-1 > Cu/Cheto-2 > Cu/Cheto-3. Considering the presence of this peak at much higher temperatures, it is assumed that the second type of adsorption sites (sites B) is located in-between the clay layers, while the first type of sites (sites A) is located on the edge or the external surface of the clay layer. During the sample preparation, most of the copper complex sits on sites A with minor amount diffuses onto sites B. When the sample is heated, the decomposition of the copper complex starts from sites A and further increasing the temperature results in the decomposition of the copper complex on sites B. It is not clear why the adsorption on sites B shows the reverse order as that on sites A, although the difference is not significant. One possible explanation is that with higher Cu / Cheto ratio, there are more copper complex adsorbed on the edge of the clay layer, which might block the entrance for the copper complex to diffuse into the gallery between the layers. The former study showed that metal ion adsorption more likely happened on the edge of the clay layers when the solution had pH higher than 10 and particularly high background electrolyte concentration [18]. Since in this work, copper adsorption was conducted under pH of 12, edge adsorption would be favoured, which supports the above assumption. As for the dehydroxylation of clay structurally bonded hydroxyl groups, all three Cu/Cheto-n samples show dehydroxylation peak with similar position and intensity as that of the original Cheto clay. Therefore, the 2:1

dioctahedral clay structure is not affected by copper adsorption. It is interesting to observe the N₂O peak during the TGA analysis. From Fig. 5, it is seen that the difference for this peak intensity among three samples is small, following the order of Cu/Cheto-2 > Cu/Cheto-1 > Cu/Cheto-3. As discussed before, it is proposed that this N₂O peak is a result of the chemical reaction between the adsorbed copper species and carrier gas, nitrogen, but not a pure thermodecomposition. If this is correct, a normal ramping at 4 °C/min might not be slow enough to let those copper species fully react with nitrogen and the results shown in Fig. 5 might be misleading. To clarify this, TGA-MS analysis was conducted again under condition II. The results are illustrated in Fig. 6 and Fig. 7 for comparison.

Fig. 6 and Fig. 7.

By comparison of Fig. 6 (a) with Fig. 7 (a), it is seen that DTGA curves for all three samples obtained under condition II follow the trends precisely as those obtained under condition I, except in region (iii) where N₂O is released. Fig. 7 (a) shows apparently higher peak intensity for Cu/Cheto-2 than Cu/Cheto-1 and Cu/Cheto-3. The corresponding MS comparison, Fig. 6 (b) and Fig. 7 (b), demonstrates the same discrepancy. Therefore, it is concluded that N₂O is coming from the reaction between copper species and nitrogen. Furthermore, not all adsorbed copper species can join this reaction. The copper loading is in the order of Cu/Cheto-3 > Cu/Cheto-2 > Cu/Cheto-1. If all the copper species are involved in this reaction, one would expect to see the N₂O peak intensity following the same order, which is not the case in this study. As mentioned before, copper is absorbed on two types of sites. However, the structure of the adsorbed copper species has not been discussed. It was reported that with increase of pH, the structure of the adsorbed copper species would change from outer-sphere complex to inner-sphere monomer or multinuclear complex and finally to dimers under high pH [18, 19].

To study the state of copper in Cu/Cheto-n samples, UV-vis DRS experiment was conducted. The results are shown in Fig. 8. The band assignments are summarized in Table 2.

Fig. 8.
Table 2.

It is seen that all the samples show multiple bands in the region of 220nm – 280nm, which are assigned to the charge transfer (CT) O→Cu transitions of isolated Cu²⁺ ions in coordination with lattice oxygen [7, 20]. Bands in 300nm – 350nm are coming from the CT O→Cu transitions of the highly dispersed copper clusters [7, 20, 21]. There were reports assigned them either to single-O-bridged copper pairs [22] or double-O-bridged copper pairs [21]. Broad band in 400nm – 450nm is CT band for either single- or double-O-bridged copper pairs [21-23]. The appearance of bands in regions (ii) and (iii) clearly indicates that part of the adsorbed copper has a dimer structure. Another broad band in 650nm – 900nm is assigned to d-d transition of Cu²⁺. If Cu²⁺ is in perfect octahedral configuration, d-d transition band will be in 750nm – 800nm [7, 8, 20, 22, 23]. If Cu²⁺ is in distorted octahedral (nearly square planar) configuration, the band will have blue shift to 600nm – 750nm. From Fig. 8, it is clear that for Cu/Cheto-n samples, Cu²⁺ is almost in octahedral configuration. As a summary, Fig. 8 shows that for all Cu/Cheto-n samples, part of the adsorbed copper is in isolated Cu²⁺ form and part of it is in agglomerated dimer form. Comparison among three samples shows that Cu/Cheto-3 has higher intensity in regions (i), (iii) and (iv), which indicates that Cu/Cheto-3 has higher amount of both isolated and agglomerated copper structure. It is believed that most of the agglomerated copper species stay on the edge or external surface of the clay layer.

Since no signal for any crystallized copper phases was detected by XRD analysis, these agglomerated copper species disperse well over the clay surface. Fig. 7 shows the highest N₂O peak for Cu/Cheto-2, suggesting there is an optimum concentration, or agglomerated degree of copper for the reaction.

The weight loss in region (iv) is coming from oxygen, which does not exist in the original Cheto clay. The intensities for this peak follow the order of Cu/Cheto-3 > Cu/Cheto-2 > Cu/Cheto-1. Since a similar peak was observed in the DTGA curve of the copper precursor, it is assigned to the reconstructing of the agglomerated copper species. The intensity change trend agrees well with the order of the copper concentration in the samples. This further supports the above discussion that all samples have agglomerated copper structure and the higher the copper concentration, the higher the agglomeration extent.

Conclusions

Copper adsorption on Cheto clay was conducted under the basic condition. The XRD results show that the original Cheto clay rehydrate easily. A clear step-by-step exchange of hydrated calcium by copper complex is presented through the DTGA-MS results. Two different types of copper adsorption sites (A and B) are determined in DTGA curves. Sites A, which are also the dominant one, locate on the edge or external surface of the clay layers. While sites B locate in-between the layers. Thermodecomposition of adsorbed copper complex happens first on sites A, corresponding to the DTGA peaks in region (ii). Further enhance the temperature results in the thermodecomposition of the adsorbed copper complex on sites B, corresponding to first part of the DTGA peaks in region (iii). With the help of MS, a kinetic reaction is distinguished from the pure thermodecomposition. The appearance of the N₂O and O₂ peaks shows that the adsorbed copper species are in agglomerated form and the higher the copper loading concentration, the higher the agglomeration extent, which is confirmed by DRS results. DTGA-MS proved to be a valuable technique to study the adsorption of copper on clay samples and monitor the structure change during heating.

Acknowledgements

The authors thank the School of Physical and Chemical Sciences, Queensland University of Technology, for the financial and infrastructure support. The Australian Research Council (ARC) is also gratefully acknowledged.

References

- [1] Luck, F., *Catal. Today* **53**, 81 (1999).
- [2] Alejandre, A., Medina, F., Fortuny, A., Salagre P., and Sueiras, J.E., *Appl. Catal. B: Environ.* **16**, 53 (1998).
- [3] Yu, J., and Savage, P.E., *Appl. Catal. B: Environ.* **28**, 275 (2000).
- [4] Alejandre, A., Medina, F., Rodriguez, X., Salagre, P., Cesteros, Y., and Sueiras, J.E., *Appl. Catal. B: Environ.* **30**, 195 (2001).
- [5] Alvarez, P.M., McLurgh, D., and Plucinski, P., *Ind. Eng. Chem. Res.* **41**, 2147 (2002).
- [6] Alvarez, P.M., McLurgh, D., and Plucinski, P., *Ind. Eng. Chem. Res.* **41**, 2153 (2002).
- [7] Montanari, B., Vaccari, A., Gazzano, M., Kabner, P., Papp, H., Pasel, J., Dziembaj, R., Makowski, W., and Lojewski, T., *Appl. Catal. B: Environ.* **13**, 205 (1997).

- [8] Komova, O.V., Simakov, A.V., Rogov, V.A., Kochubei, D.I., Odegova, G.V., Kriventsov, V.V., Paukshtis, E.A., Ushakov, V.A., Sazonova, N.N., and Nikoro, T.A., *J. Molecular Catal. A: Chem.* **161**, 191 (2000).
- [9] Wang, X., Hou, W., Wang, X., and Yan, Q., *Appl. Catal. B: Environ.* **35**, 185 (2002).
- [10] Bahranowski, K., Gasior, M., Kielski, A., Podobinski, J., Serwicka, E.M., Vartikian, L.A., and Wodnicka, K., *Clays and Clay Minerals* **46**, 98 (1998).
- [11] Barrault, J., Bouchoule, C., Echachoui, K., Frini-Srasra, N., Trabelsi, M., and Bergaya, F., *Appl. Catal. B: Environ.* **15**, 269 (1998).
- [12] Li, W., Sirilumpen, M., and Yang, R.T., *Appl. Catal. B: Environ.* **11**, 347 (1997).
- [13] Yang, R.T., Tharappiwattananon, N., and Long, R.Q., *Appl. Catal. B: Environ.* **19**, 289 (1998).
- [14] Sirilumpen, M., Yang, R.T., and Tharapiwattananon, N., *J. Molecular Catal. A: Chem.* **137**, 273 (1999).
- [15] Bahranowski, K., Kielski, A., Serwicka, E.M., Wisla-Walsh, E., and Wodnicka, K., *Microporous Mesoporous Mater.* **41**, 201 (2000).
- [16] Ding, Z., Klopogge, J.T., and Frost, R.L., *J. Porous Mater.* **8**, 273 (2001).
- [17] Rojas-Hernandez, A., Ramirez, M. T., Gonzalez, I., and Ibanez, J. G., *J. Chem. Educ.* **72**, 1100 (1995).
- [18] Morton, J.D., Semrau, J.D., and Hayes, K.F., *Geochimica et Cosmochimica Acta* **65**, 2709 (2001).
- [19] Hyun, S.P., Cho, Y.H., Kim, S.J., and Hahn, P.S., *J. Colloid & Interface Sci.* **222**, 254 (2000).
- [20] Teraoka, Y., Tai, C., Ogawa, H., Furukawa, H., and Kagawa, S., *Appl. Catal. A* **200**, 167-176 (2000).
- [21] Groothaert, M. H., Bokhoven, J. A. van, Battiston, A. A., Weckhuysen, B. M., and Schoonheydt, R. A., *J. Am. Chem. Soc.* (Published on Web).
- [22] Praliaud, H., Mikhailenko, S., Chajar, Z., and Primet, M., *Appl. Catal. B: Environ.* **16**, 359-374 (1998).
- [23] Carvalho, M.C.N.A.de, Passos, F. B., and Schmal, M., *Appl. Catal. A* **193**, 265-276 (2000).

List of Tables:

Table 1. Bulk element concentrations for different samples.

Table 2. UV-vis DRS band assignments for Cu/Cheto-n samples.

List of Figures:

Fig. 1. XRD patterns of original Cheto and Cu/Cheto-n samples.

(a) Freshly prepared. (b) Calcined at 400 °C

Fig. 2. XRD patterns of original Cheto clay after calcination (400 °C) and left in air, from bottom, for 0.5 h, 1 h, 12 h, 1 month and Cheto clay without calcination.

Fig. 3. DTGA-MS (analysis condition I) results for original Cheto clay.

Fig. 4. DTGA-MS (analysis condition I) results for Cu/Cheto-2.

Fig. 5. Comparison of DTGA (analysis condition I) results for different Cu/Cheto-n samples.

Fig. 6. DTGA-MS (analysis condition I) results for Cu/Cheto-n samples.

(a) DTGA (replot on large scale). (b) MS for mass 44.

Fig. 7. DTGA-MS (analysis condition II) results for Cu/Cheto-n samples.

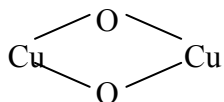
(a) DTGA. (b) MS for mass 44.

Fig. 8. UV-vis DRS spectra of Cu/Cheto-n samples.

Table 1. Bulk element concentrations for different samples.

| Sample | SiO ₂ (wt%) | Al ₂ O ₃ (wt%) | MgO (wt%) | CaO (wt%) | CuO (wt%) |
|------------|------------------------|--------------------------------------|-----------|-----------|-----------|
| Cheto | 62 | 21 | 6.5 | 2.7 | 0 |
| Cu/Cheto-1 | 63 | 19 | 5.4 | 2.0 | 1.5 |
| Cu/Cheto-2 | 63 | 20 | 5.6 | 0.55 | 4.0 |
| Cu/Cheto-3 | 64 | 21 | 4.7 | 0 | 5.3 |

Table 2. UV-vis DRS band assignments for Cu/Cheto-n samples.

| Band range (nm) | Band position (nm) | | | Transitions |
|--------------------|--------------------|------------|------------|--|
| | Cu/Cheto-1 | Cu/Cheto-2 | Cu/Cheto-3 | |
| (i) 220–280 | 220 | | 220 | CT O→Cu transitions |
| | 230 | 225 | 230 | |
| | 245 | 243 | 249 | |
| | 270 | 272 | 269 | |
| (ii) 300–350 | 310 | 310 | 307 | CT O→Cu transitions |
| | 325 | 325 | 330 | |
| | 342 | 342 | 342 | |
| (iii) 400–450 | | 400 – 450 | | CT Cu–O–Cu or  transitions |
| (iv) 650–900 | | 650-900 | | d-d transitions of Cu ²⁺ |

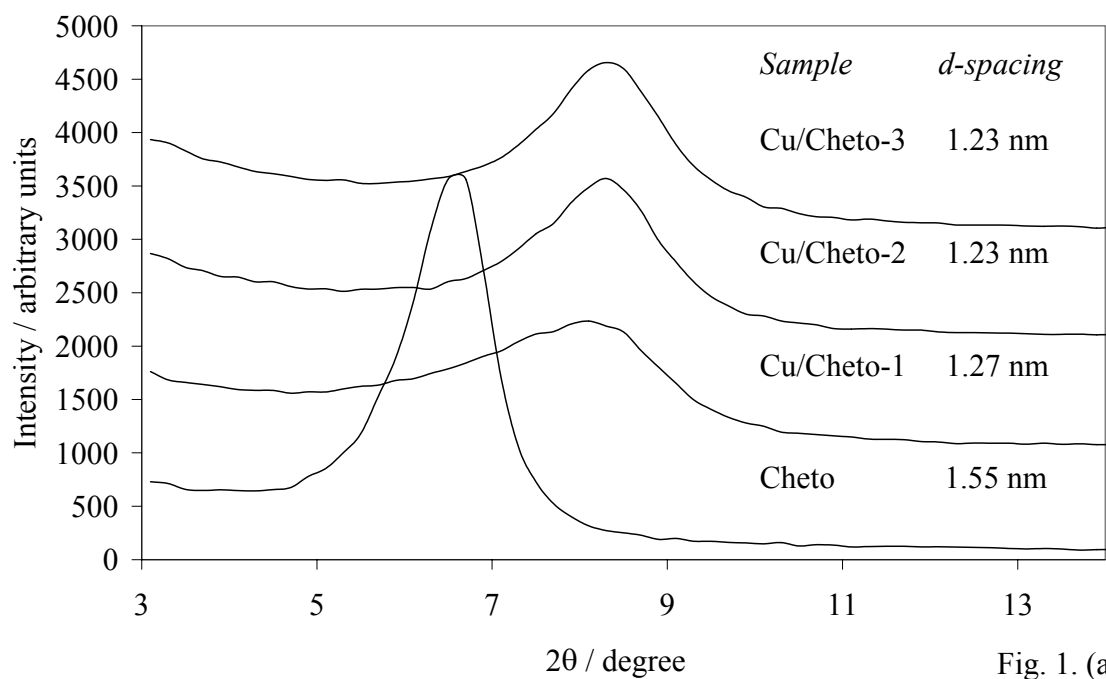


Fig. 1. (a)

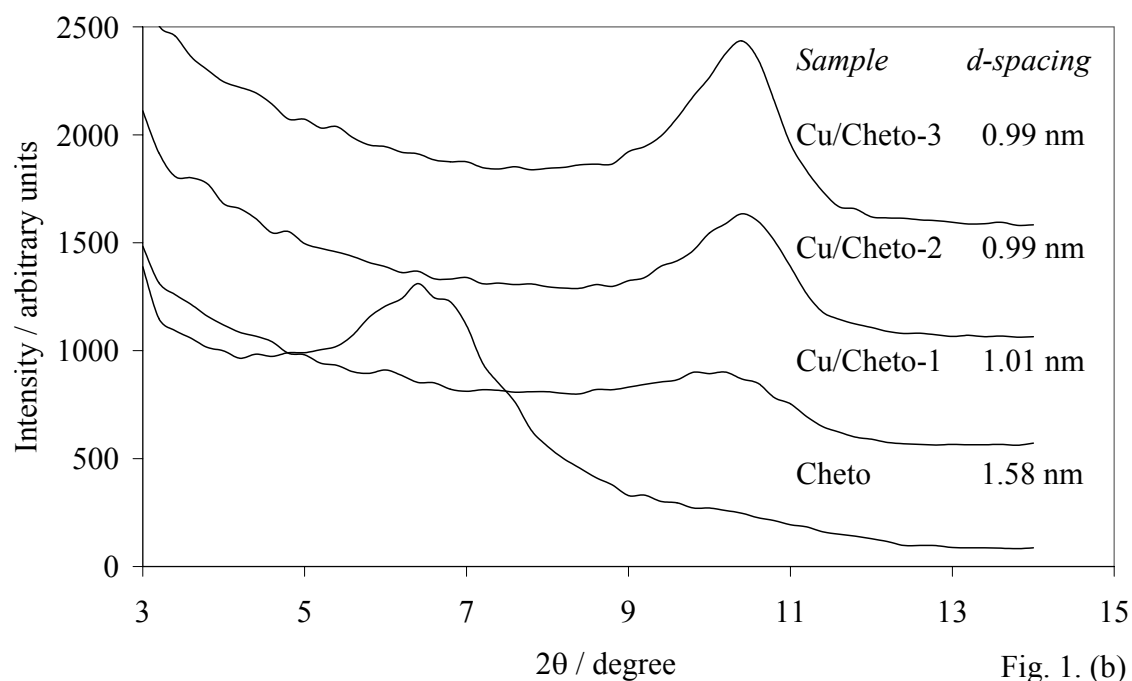
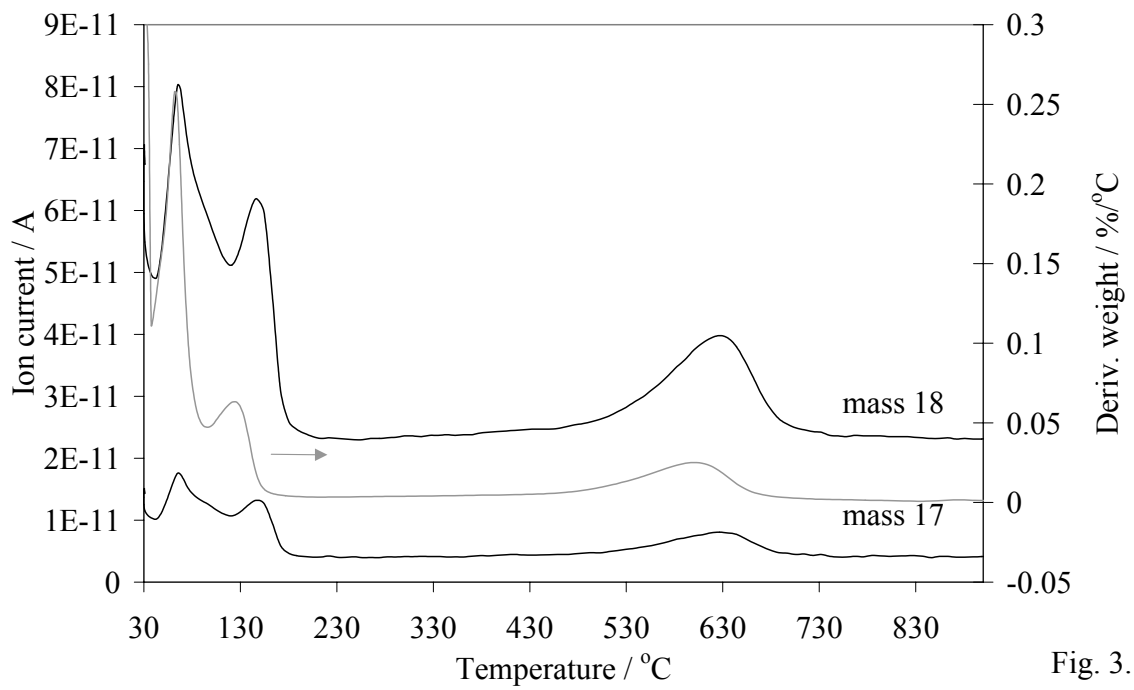
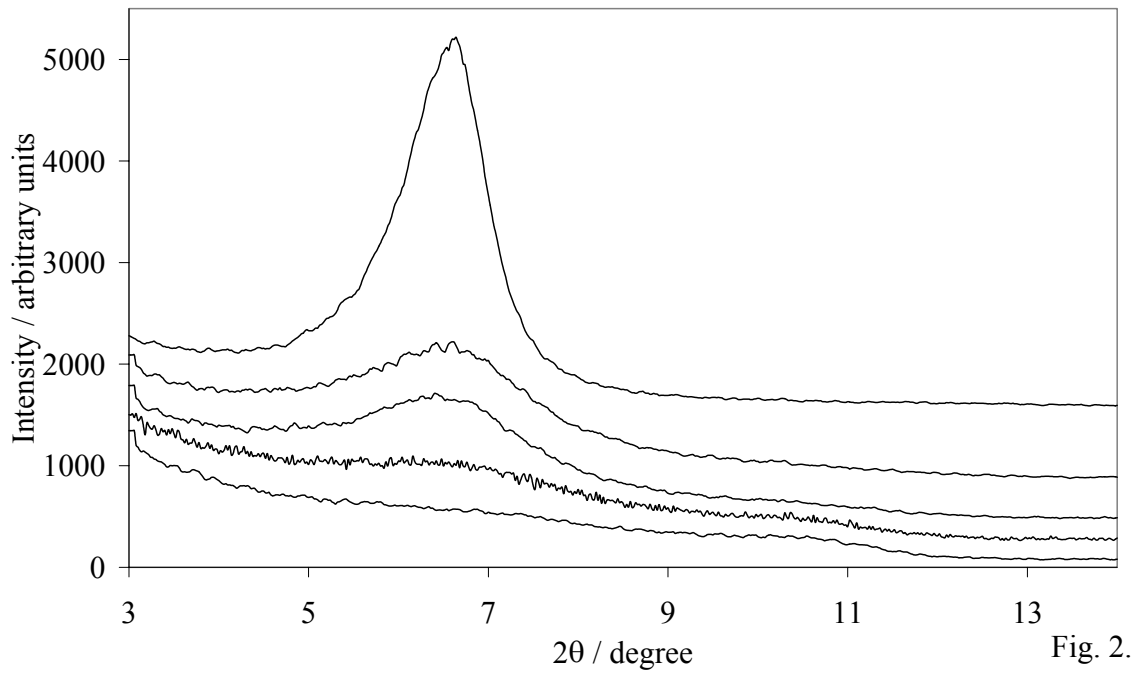


Fig. 1. (b)



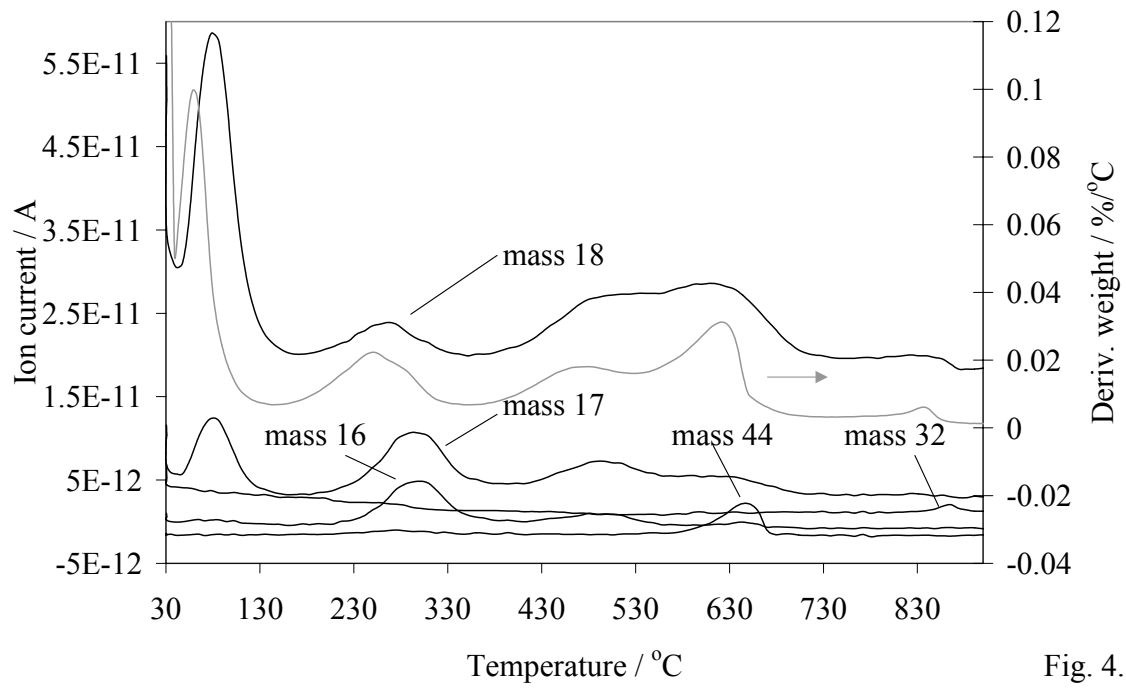


Fig. 4.

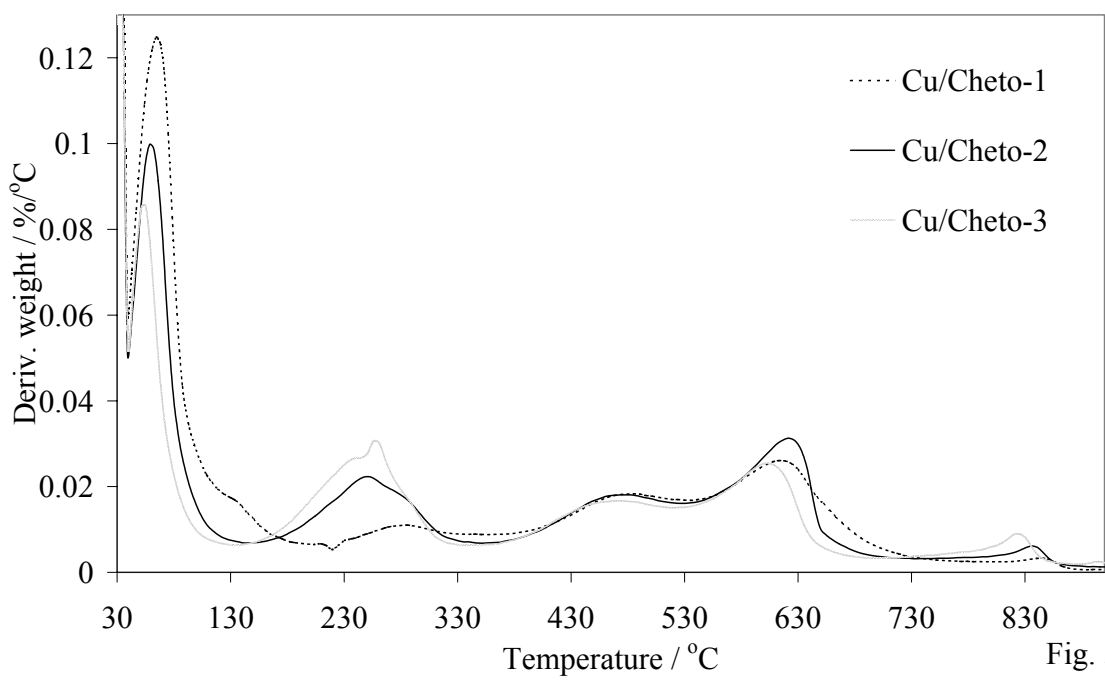


Fig. 5.

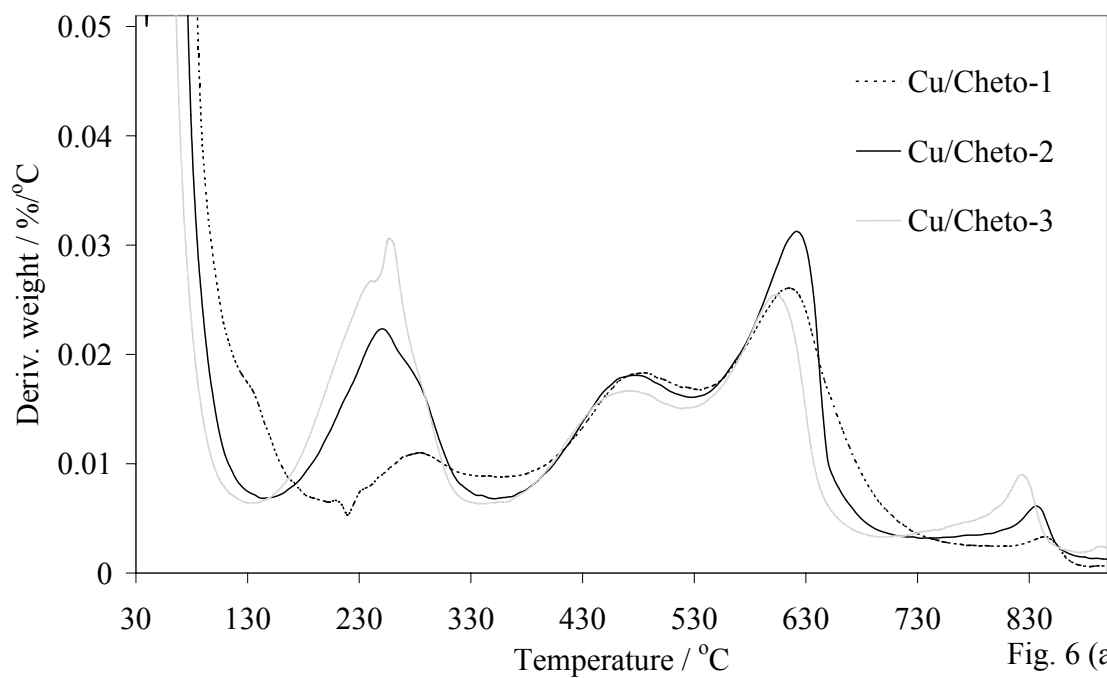


Fig. 6 (a).

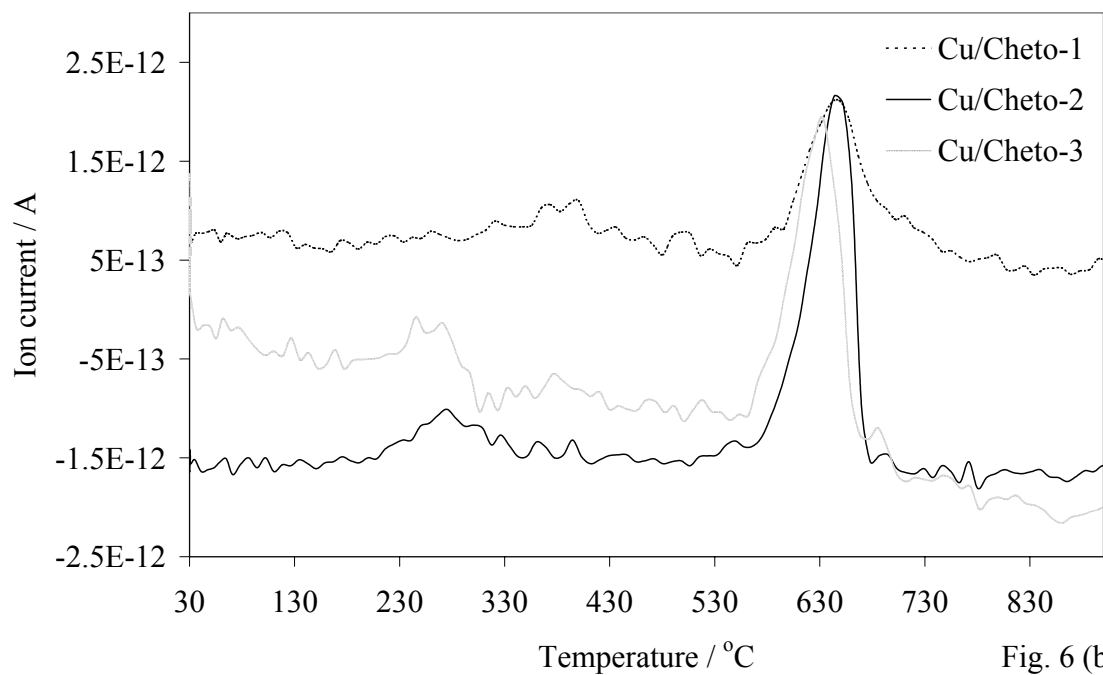
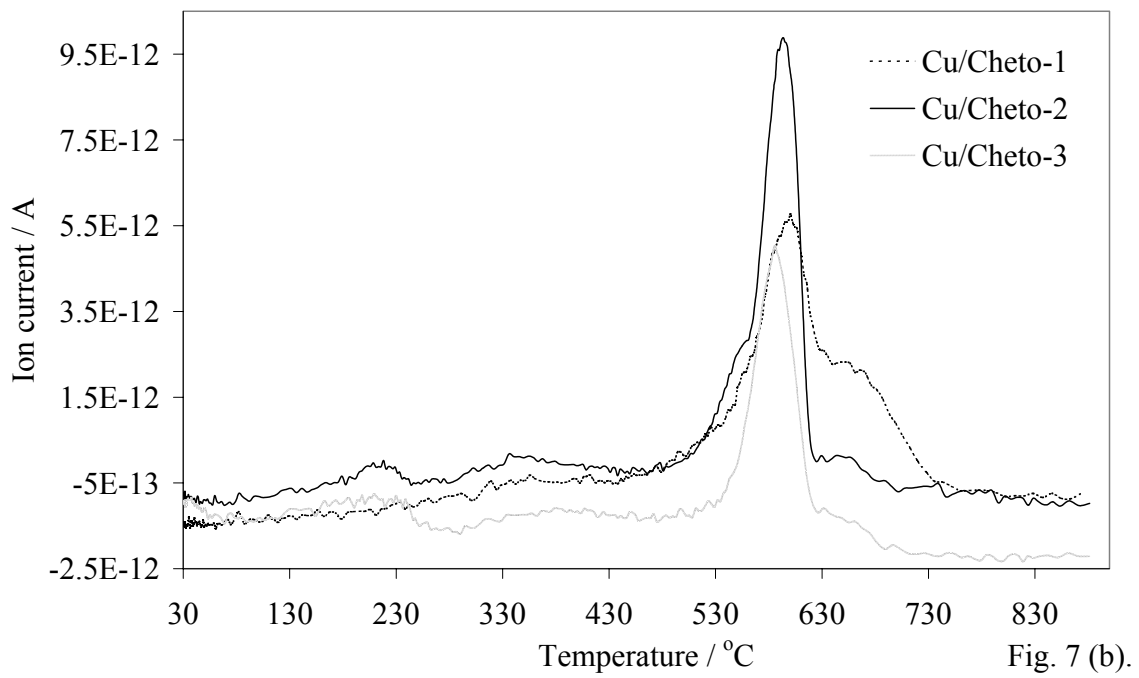
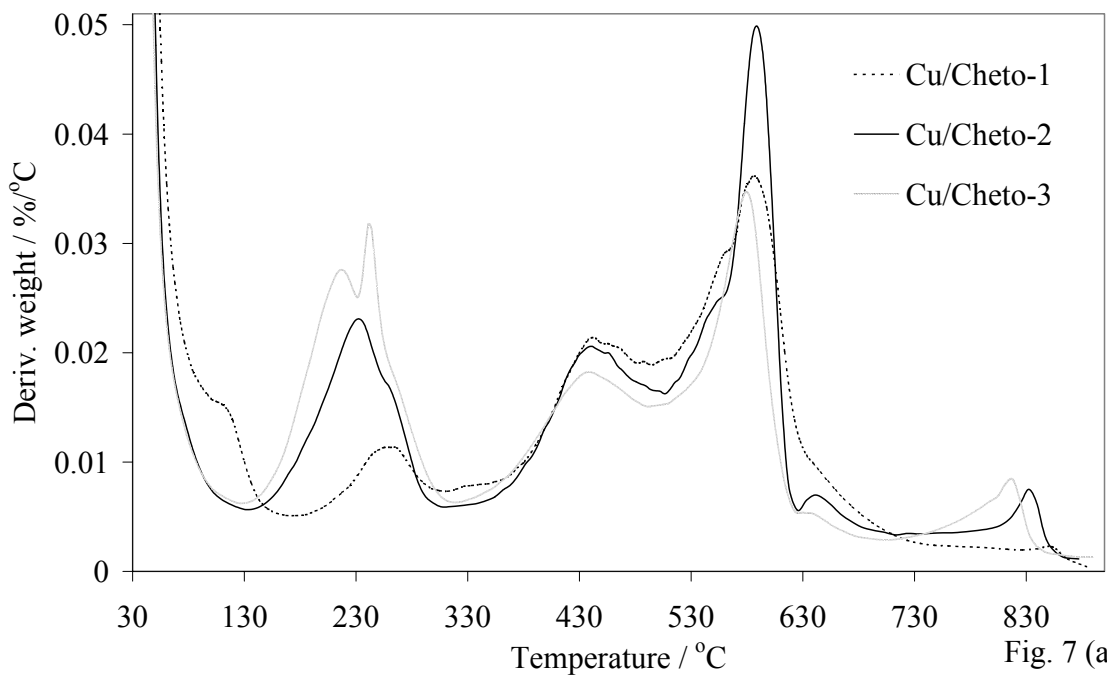


Fig. 6 (b).



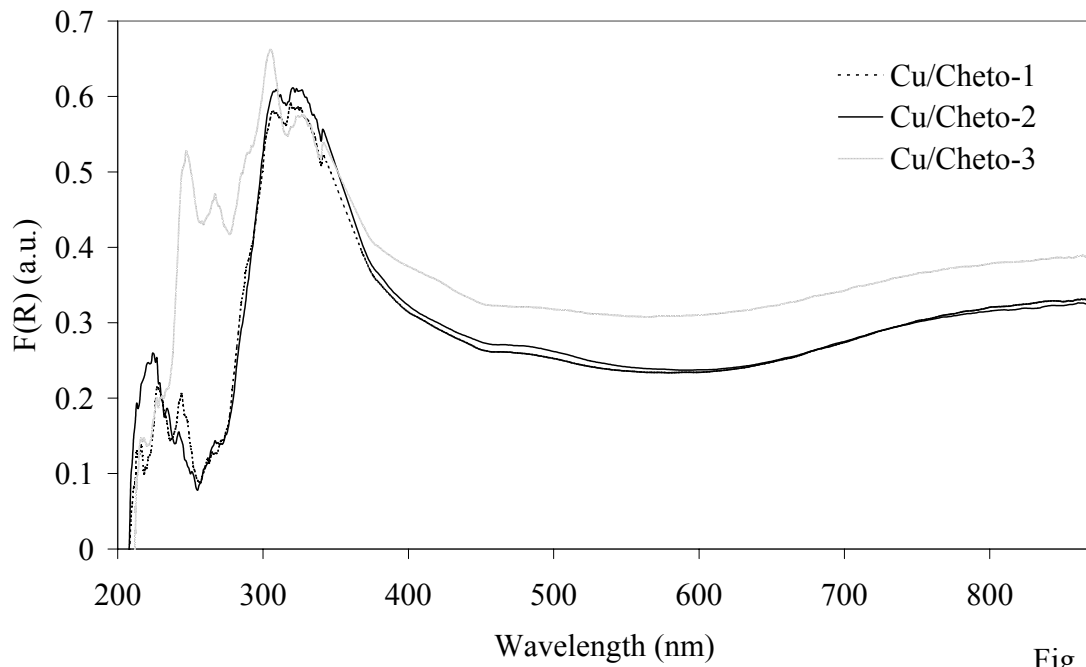


Fig. 8.